Paleoclassical model for edge electron temperature pedestal

J.D. Callen*
University of Wisconsin, Madison, WI 53706-1609

T.H. Osborne, R.J. Groebner, H.E. St. John
General Atomics, San Diego, CA 92186-5608

A.Y. Pankin, G. Bateman, A.H. Kritz
Lehigh University, Bethleham, PA 18015-3182

W.M. Stacey
Georgia Tech, Atlanta, GA 30332

(Dated: March 22, 2007)

A model is proposed for the edge electron temperature profile $T_e(\rho)$ in high (H) confinement mode, diverted tokamak plasmas based on the paleoclassical model for the minimum radial electron heat transport. Moving inward from the separatrix, T_e profile predictions are: first an increasing T_e gradient with $\eta_e \equiv d\ln T_e/d\ln n_e \simeq 2$, a maximum $|\boldsymbol{\nabla} T_e|$ where q drops to $\lesssim 5$, then a decreasing $|\boldsymbol{\nabla} T_e|$, and finally a pedestal electron pressure determined by balancing collisional paleoclassical transport against gyro-Bohm-scaled anomalous electron heat transport: $p_e^{\rm ped} \equiv n_e^{\rm ped} T_e^{\rm ped} \propto (\bar{a}/\bar{R}q)B^2$. Model predictions and transport modeling with it compare well with pedestal data from DIII-D.

PACS numbers: 52.55.Dy, 52.55.Fa, 52.25.Fi, 52.40.Hf

Overall plasma confinement in tokamaks is composed of two parts: core (normalized radius $\rho \lesssim 0.9$) and edge ($0.9 \lesssim \rho \lesssim 1$) confinement. It is determined to a large degree in high (H-) confinement mode diverted plasmas by plasma transport in the edge, and in particular by the "pedestal" pressure $p^{\rm ped}$ (and hence temperature $T^{\rm ped}$) at the top of the edge pedestal, at the transition to the core region. For example, predictions for fusion plasma performance in the planned international ITER experiment [1] scale as $(T^{\rm ped})^{1.8}$ at fixed pedestal density [2].

Plasma transport in the edge of diverted H-mode plasmas involves many processes. The density profile inside the magnetic separatrix is determined primarily [3, 4] by balancing neutral fueling and radial particle transport. The total pedestal pressure (or edge radial pressure gradient) is limited by macroscopic peeling-ballooning instabilities that cause edge localized modes (ELMs) [5].

Here, we focus on electron heat transport in the edge of an H-mode plasma, which is currently not understood. Anomalous plasma transport induced by drift-wave-type microturbulence is usually scaled to the gyroBohm diffusion coefficient $D^{\rm gB} \sim (\varrho_S/a)(T_e/eB) \propto T_e^{3/2}/aB^2$; hence, it could be small in the edge where T_e is low. Also, fluctuations are usually reduced in H-mode plasmas [6]; hence, the anomalous transport they induce could be small in H-mode pedestals. In contrast, the paleoclassical electron heat diffusivity [7–9] $\chi_e^{\rm pc} \propto a^{1/2} T_e^{-3/2}$ increases as T_e decreases. Thus, for $T_e \lesssim T_e^{\rm crit} \simeq B({\rm T})^{2/3}\bar{a}({\rm m})^{1/2}$ keV [10] paleoclassical electron heat transport could be dominant, i.e., in the edge pedestals of H-mode plasmas.

In this paper we develop and test against pedestal data from DIII-D [11] a model for the edge electron temperature profile $T_e(\rho)$ and pedestal pressure $p_e^{\rm ped}$ based on the hypothesis that paleoclassical electron heat transport [7, 8] is dominant in an H-mode pedestal. Key model assumptions are: 1) In a "near transport equilibrium" state between Type I (large, long repetition time) ELMs, electron heat transport is dominated by paleoclassical radial electron heat transport [7, 8] in the edge pedestal. 2) The electron temperature on the divertor separatrix is fixed [12] — by balancing heat flow across the separatrix against parallel electron heat conduction on open field lines outside it. And 3) the edge electron density profile is fixed, and in particular given by the hyperbolic tangent form proposed by Porter *et al.* [12] whose characteristic width is labeled [3, 4] Δ_n (typically $\sim$ cm) and whose radial position of the inflection point in the edge density profile (where $|\boldsymbol{\nabla} n_e|$ is maximum) is ρ_n.

Then, the steady-state electron energy balance is [7, 8]

$$Q_e = \frac{\partial}{\partial V}\langle \mathbf{Q}_e^{\rm pc}\boldsymbol{\cdot}\boldsymbol{\nabla} V\rangle \equiv -\frac{M+1}{V'}\frac{d^2}{d\rho^2}\left(V'\frac{D_\eta}{\bar{a}^2}\frac{3}{2}n_e T_e\right). \quad (1)$$

Here, Q_e is the net electron heating power per unit volume (direct heating plus collisional heating from ions minus convection and radiation losses) and $\langle \mathbf{Q}_e^{\rm pc}\boldsymbol{\cdot}\boldsymbol{\nabla} V\rangle$ is the radial electron heat flow induced in resistive, current-carrying toroidal plasmas by the paleoclassical processes of electron guiding centers and heat being transported along with thin poloidal flux annuli diffusing radially with the magnetic field diffusivity $D_\eta \equiv \eta_\parallel^{\rm nc}/\mu_0$ [7, 8]:

$$\chi_e^{\rm pc} \simeq \frac{3}{2}(M+1)D_\eta, \;\; D_\eta \simeq \frac{\eta_\parallel^{\rm nc}}{\eta_0}\frac{1400\,Z}{[T_e({\rm eV})]^{3/2}}\,\frac{{\rm m}^2}{\rm s}, \quad (2)$$

where $Z \to Z_{\rm eff} \equiv \sum_i n_i Z_i^2/n_e$ is the effective ion charge.

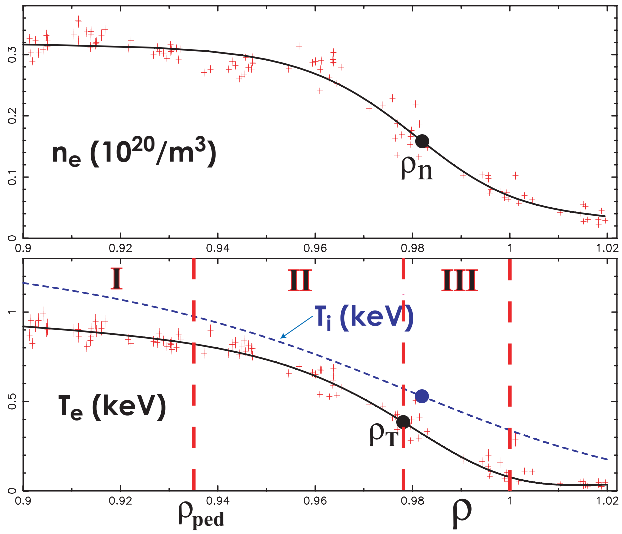

FIG. 1: "Equilibrium" n_e, T_e pedestal profiles for DIII-D H-mode shot 98889, averaged over 80–99% of time ($\sim$ 36 ms) to next ELM crash, around 4500 ms. The lines show tanh fits to Thomson scattering data with symmetry points at ρ_n, ρ_T.

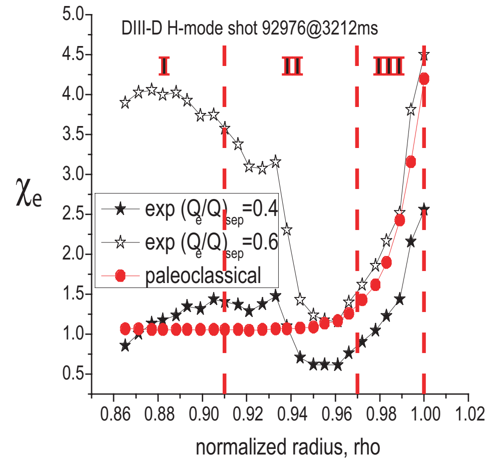

FIG. 2: Interpretive [16] profile of χ_e, $\chi_e^{\rm pc}$ (m^2/s) in pedestal similar to Fig. 1. Agreement in edge (II,III) is reasonable since uncertainties in both χ_e values are $\gtrsim$ 2. $(Q_E/Q)_{\rm sep}$ is assumed electron fraction of power flow through separatrix.

The ratio of the neoclassical parallel resistivity $\eta_\parallel^{\rm nc}$ to the reference (perpendicular) resistivity $\eta_0 \equiv m_e \nu_e / n_e e^2 \simeq 1400\, Z/[T_e({\rm eV})]^{3/2}$ is given approximately by [7, 8]

$$\eta_\parallel^{\rm nc}/\eta_0 \simeq 0.43 + 2\,/\,(1 + \nu_{*e}^{1/2} + \nu_{*e}) \qquad (3)$$

for DIII-D [11] edge plasmas where $Z_{\rm eff} \sim 2$. Here, $\nu_{*e} \equiv R_0 q/(\epsilon^{3/2}\lambda_e)$ is the neoclassical electron collisionality parameter with electron collision length $\lambda_e \simeq 1.2 \times 10^{16} [T_e({\rm eV})]^2/(n_e Z)$ m and $\epsilon \equiv r/R_0 \simeq 0.4$ is the DIII-D edge inverse aspect ratio. For edge plasmas the paleoclassical helical multiplier M is [7, 8, 10]

$$M \simeq \frac{1}{\pi \bar{R} q\,/\lambda_e + 1/n_{\max}}, \quad n_{\max} \equiv \frac{1}{(\pi \bar{\delta}_e q')^{1/2}}, \qquad (4)$$

in which $\bar{R} \simeq R_0$ is an average major radius, $\bar{\delta}_e \equiv (c/\omega_p \bar{a})$ is a normalized electromagnetic skin depth and $q' \equiv |dq/d\rho|$. Also, ρ is a toroidal-flux-based dimensionless radial variable, $V' \equiv dV/d\rho \propto \rho$ is the radial derivative of the volume of a flux surface, and $\bar{a} \simeq a\,[2\kappa^2/(1+\kappa^2)]^{1/2}$ is a (paleoclassical) average radius for a plasma with nominal minor radius a (half-width in horizontal midplane) and cross-section ellipticity $\kappa = b/a$. These and other symbols in (1)–(4) are defined precisely in [7, 8].

Figure 1 shows typical "equilibrium" electron density and temperature profiles in a DIII-D low density H-mode pedestal. As indicated, the T_e profile will be characterized by three regions [10] — III ($\rho_T < \rho < 1$): from separatrix inward to the T_e inflection point $\rho_T \simeq 0.978$, II ($\rho_{\rm ped} < \rho < \rho_T$): from T_e inflection point to top of T_e pedestal defined here as the point $\rho_{\rm ped} \simeq \rho_T - \Delta_T \simeq 0.935$ where tanh $2 \simeq 0.964$, and III ($\rho < \rho_{\rm ped}$): from top of T_e pedestal inward to the hot core plasma.

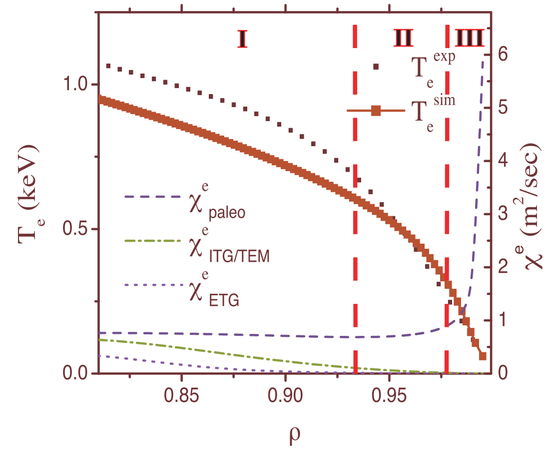

FIG. 3: ASTRA modeling (500 radial points) [18] of $T_e(\rho)$ in H-mode edge pedestal like that in Fig. 1. Diffusivities due to ion-temperature-gradient/trapped-electron and electron-temperature-gradient microinstabilities are $\chi^e_{\rm ITG/TEM}$ and $\chi^e_{\rm ETG}$. Edge (regions II,III) T_e profile is determined by $\chi_e^{\rm pc}$.

The "power balance" electron heat diffusivity χ_e obtained from interpretive transport modeling [16] is compared with the $\chi_e^{\rm pc}$ defined in (1)–(4) in Fig. 2. Figure 3 shows predictive modeling of the edge T_e profile for parameters close to those in 98889 using the ASTRA code [18]; it indicates the transition from region II to I is where anomalous diffusion induced by microturbulence begins to be a significant fraction of the paleoclassical $\chi_e^{\rm pc}$. Similar χ_e profiles for other H-mode pedestals are shown in Refs. [15–17]; χ_e and $\chi_e^{\rm pc}$ agree in most but not all "equilibrium" cases in regions II (partially) and III (mostly). Paleoclassical transport in these three regions and the resultant pedestal $T_e(\rho)$ predictions will now be discussed.

Region III: Inside but near the magnetic separatrix in diverted plasmas q becomes very large and the paleoclassical helical multiplier M becomes about unity or less:

$$M \lesssim 1 \ \text{for} \ \lambda_e \lesssim \pi \bar{R} q, \quad \text{region III: } \rho_T < \rho < 1. \quad (5)$$

At ρ_T in Fig. 1, $M \simeq 1.8$; but $M \propto T_e^2/n_e q$ decreases rapidly for $\rho > \rho_T$ and $M < 1$ for $\rho \gtrsim 0.985$. In this region ν_{*e} is large and the neoclassical resistivity reduces to the Spitzer resistivity $\eta_\parallel^{\rm Sp}$ — first term on right of (3). Thus, close to the separatrix the paleoclassical electron heat diffusivity becomes [7, 8] $\chi_{es}^{\rm pc} \simeq (3/2)\, \eta_\parallel^{\rm Sp}/\mu_0$ or

$$\chi_{e\rm III}^{\rm pc} \simeq \frac{900\, Z}{[T_e({\rm eV})]^{3/2}} \, \frac{\rm m^2}{\rm s}, \quad \text{region III: } \rho_T < \rho < 1. \quad (6)$$

Since $\chi_e \simeq \chi_e^{\rm pc}$ decreases as T_e increases inside the separatrix, we infer from a Fourier heat flux relation $\mathbf{q}_e \simeq -\,n_e \chi_e \boldsymbol{\nabla} T_e$ that $|\boldsymbol{\nabla} T_e|$ should increase for decreasing ρ. Thus, in region III $T_e(\rho)$ should have positive or neutral curvature ($d^2 T_e/d\rho^2 \geq 0$), as is evident in Fig. 1 and is usually observed experimentally in H-mode plasmas. The rapid increase of $\chi_e^{\rm pc}$ with ρ here is critical for obtaining $\partial^2 T_e/\partial \rho^2 \geq 0$ in this region, as indicated in Fig. 3. [An alternate, UEDGE model [12] uses constant χ_e in region III; it attributes the increasing χ_e toward the separatrix to parallel heat conduction toward the divertor X-point.]

Integrating (1) from the separatrix inward over the volume of the radial (ρ) region where $M << 1$ and neglecting the local electron heating in this region (i.e., $\int_\rho^1 V' d\rho\, Q_e$), we obtain the electron heat flow relation $-\,(d/d\rho)[V'(D_\eta/\bar{a}^2)(3/2) n_e T_e]_\rho = \langle \mathbf{Q}_e^{\rm pc} \boldsymbol{\cdot} \boldsymbol{\nabla} V \rangle_{\rm sep}$. Here, the right side represents the (paleoclassical) radial electron heat flow across the separatrix. Integrating this equation from ρ to the separatrix at $\rho = 1$, neglecting this electron heat flow "boundary condition," whose effect is small for a thin Region III (i.e., for $1 - \rho_T << 1$), and using (6) which implies $n_e D_\eta T_e \propto n_e T_e^{-1/2}$ yields

$$\frac{T_e(\rho)}{T_e(1)} \simeq \left[\frac{n_e(\rho)}{n_e(1)} \, \frac{V'(\rho)/\bar{a}^2(\rho)}{V'(1)/\bar{a}^2(1)} \, \frac{Z(\rho)}{Z(1)} \right]^2 \simeq \left[\frac{n_e(\rho)}{n_e(1)} \right]^2. \quad (7)$$

Thus, T_e is predicted to scale like n_e^2 in region III — to keep electron heat flow nearly constant through this region. This prediction agrees with H-mode pedestal data from ASDEX-Upgrade [13]; it also predicts [13] that in region III the ratio of electron temperature gradient to electron density gradient $\eta_e \equiv d\ln T_e/\,d\ln n_e \simeq 2$. If the electron heat flow increases (decreases) slightly with ρ, the predicted $\eta_e < 2$ (> 2). Studies in DIII-D based on the ratio of the density to temperature gradient scale

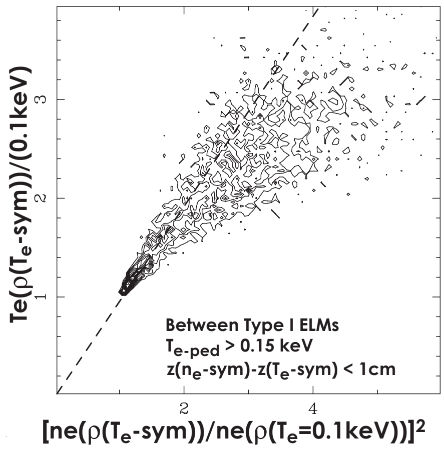

FIG. 4: Probability contours from DIII-D pedestal database (9104 points) of T_e versus n_e^2 at ρ_T, referenced to their values at the point where T_e is 0.1 keV. Dashed line indicates $\eta_e = 2$.

lengths at the symmetry point ρ_T of the pedestal T_e profile tanh fit found $\eta_e \sim$ 1–3 [14].

Figure 4 plots (7) for DIII-D pedestal data during the period between ELM crashes. Here, the $\rho = 1$ "separatrix" is defined by where $T_e \simeq 100$ eV. These data are consistent with the paleoclassical prediction of $\eta_e \simeq 2$ for $T_e \lesssim 0.2$ keV, and bounded by it for higher T_e. (The $\rho = 1$ position can be any position within Region III; we choose it to be where $T_e \simeq 100$ eV $\gtrsim T_e^{\rm sep}$ — because it is difficult to locate the separatrix precisely.)

Region II: At and inside the inflection point $\rho = \rho_T$ the helical multiplier $M \simeq \lambda_e/\pi \bar{R} q$ is usually greater than unity and the effective paleoclassical electron heat diffusivity is in its collisional (Alcator scaling) regime [7, 8]:

$$\chi_{e\rm II}^{\rm pc} \simeq \frac{3}{2} \frac{\eta_\parallel^{\rm nc}}{\eta_0} \frac{v_{Te}}{\pi \bar{R} q} \frac{c^2}{\omega_p^2}, \quad \text{region II: } \rho_{\rm ped} < \rho \lesssim \rho_T. \quad (8)$$

Moving inward from the inflection point (ρ_T), the effective $\chi_e^{\rm pc} \propto T_e^{1/2}/n_e q$ decreases slowly, as indicated in Figs. 2 and 3. This causes $|\boldsymbol{\nabla} T_e|$ to decrease [16, 17] as we move inside ρ_T — because in moving inward n_e is increasing and the electron heat flow $\langle \mathbf{q}_e \boldsymbol{\cdot} \boldsymbol{\nabla} V \rangle$ is decreasing. There is no simple way to estimate the T_e profile in region II.

Anomalous transport due to drift-wave-type microinstabilities is usually predicted to scale with the gyro-Bohm coefficient $D^{\rm gB} \simeq (\rho_S/\bar{a})(T_e/eB) \propto T_e^{3/2}/\bar{a}B^2$, albeit with a threshold-type coefficient that depends on many local quantities — magnetic shear, T_e/T_i, ν_{*e} etc. We will assume that the electron heat diffusivity induced by such microturbulence can be written as a multiple $f_\#$ ~ 1 (for electron heat transport) of this diffusivity:

$$\chi_e^{\rm gB} \simeq 3.2\, f_\# \, \frac{[T_e({\rm keV})]^{3/2} A_i^{1/2}}{\bar{a}({\rm m})\, B(T)^2} \, \frac{\rm m^2}{\rm s}, \ \text{ gyro-Bohm } \chi_e. \quad (9)$$

Here, A_i is the atomic mass ($= 2$ for deuterium).

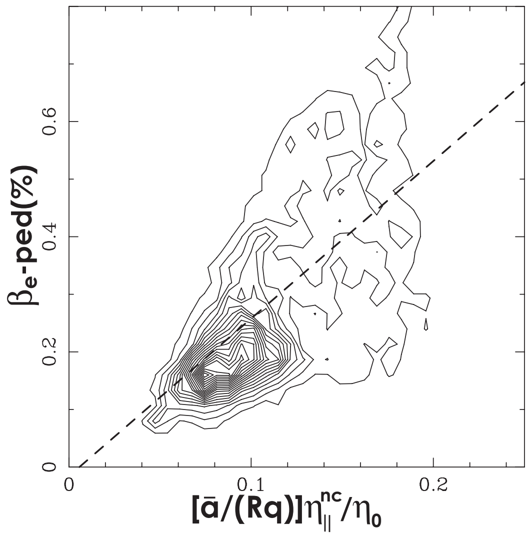

FIG. 5: Probability contours from DIII-D "between ELM crashes" pedestal database shows $\beta_e^{\rm ped}$ varies roughly linearly (dashed line is linear fit to data) with paleoclassical variable. This figure is to be reprinted from [10] with permission.

Because microturbulence-induced transport typically dominates in the hot core plasma and has a threshold-type behavior, whereas paleoclassical transport may dominate in the edge and varies smoothly, we hypothesize that the pedestal height is determined by the transition (at $\rho \sim 0.85$ in Fig. 3) between these two transport processes. Presuming paleoclassical transport is in its collisional regime ($\chi_{eII}^{\rm pc}$), the pedestal electron pressure can be estimated by equating the paleoclassical coefficient in (8) to an anomalous $\chi_e^{\rm gB}$ of the form given in (9):

$$p_e^{\rm ped} \equiv n_e^{\rm ped} T_e^{\rm ped} \simeq \frac{0.032}{f_{\#} A_1^{1/2}} \frac{\bar{a}}{\bar{R}q} \frac{\eta_{\parallel}^{\rm nc}}{\eta_0} \frac{B^2}{2\mu_0} \propto B_p B. \qquad (10)$$

This scaling yields $\beta_e^{\rm ped} \simeq (0.023/f_{\#})(\bar{a}/R_0 q)(\eta_{\parallel}^{\rm nc}/\eta_0)$ for deuterium. Figure 5 shows this prediction is consistent with the DIII-D pedestal database in both scaling [$f_{\#} \simeq 0.82$ for slope in (10)] and magnitude ($0.6 \lesssim f_{\#} \lesssim 2$).

This scaling is however quite similar to the peeling-ballooning instability criterion [5] times a fixed pedestal width, and it is questionable if it can be distinguished from it. The philosophy of the model developed here is that the pedestal T_e profile and pressure $p_e^{\rm ped}$ are quickly equilibrated by paleoclassical electron heat transport in the H-mode pedestal. Then, the edge current density and other (e.g., n_e and T_i) profiles continue evolving slowly, which eventually induces a peeling-ballooning instability thereby causing the next ELM crash.

Region I: In this region paleoclassical transport is often in its collisionless regime ($\lambda_e > \pi \bar{R} q n_{\rm max}$) where $\chi_{eI}^{\rm pc} \simeq (3/2) n_{\rm max} D_\eta$. However, since for low density H-mode plasmas usually $T_e \gtrsim T_e^{\rm crit} \simeq B^{2/3} \bar{a}^{1/2} (3 f_{\#})^{-1/3}$ keV [10] (~ 1 keV using $f_{\#} \simeq 0.82$ inferred from Fig. 5 for the DIII-D shot in Fig. 1), anomalous electron heat transport due to microturbulence usually dominates over paleoclassical transport deep in region I (i.e., for $\rho < 0.85$ in Fig. 3). (In ITER [1] $T_e^{\rm crit} \sim 3.5$–5 keV.)

The paleoclassical model for H-mode T_e pedestals compares well with DIII-D data in three important regards: 1) positive or neutral T_e profile curvature and $\eta_e \simeq 2$ in region III, 2) $\chi_e^{\rm pc}(\rho)$ and modeled $T_e(\rho)$ in regions III and (less so) II, and 3) $\beta_e^{\rm ped}$ prediction from (10) due to change from collisional paleoclassical to microturbulence-induced anomalous transport near transition from region II to I. Similar tests on pedestals in other H-mode tokamak plasmas are needed to determine how limited or universal these conclusions are, and perhaps to separate effects of paleoclassical transport and peeling-ballooning instabilities (ELMs) whose scalings are quite similar.

The authors gratefully acknowledge useful discussions with M.A. Mahdavi and P.B. Snyder, and the careful reading and critique of the original manuscript by C.C. Petty which resulted in significant improvements of it. This research was supported by DoE grants and contracts DE-FG02-92ER54139 (UW-Madison), DE-FC02-04ER54698 (GA), DE-FG02-92ER54141 (Lehigh), and DE-FG02-00ER54538 (Georgia Tech).

* `callen@engr.wisc.edu`; `www.cae.wisc.edu/~callen`

[1] R. Aymar *et al.*, Nucl. Fusion **41**, 1301 (2001).
[2] J.E. Kinsey *et al.*, Nucl. Fusion **43**, 1845 (2003).
[3] M.A. Mahdavi *et al.*, Nucl. Fusion **42**, 52 (2002).
[4] R.J. Groebner *et al.*, Nucl. Fusion **44**, 204 (2004).
[5] P.B. Snyder, H.R. Wilson, T.H. Osborne and A.W. Leonard, Plasma Phys. Control. Fusion **46**, A131 (2004).
[6] K.H. Burrell, Phys. Plasmas **6**, 4418 (1999).
[7] J.D. Callen, Nucl. Fusion **45**, 1120 (2005).
[8] J.D. Callen, Phys. Plasmas **12**, 092512 (2005)
[9] J.D. Callen, "Derivation of paleoclassical key hypothesis," UW-CPTC 06-8R, January 2007 (to be published in Phys. Plasmas).
[10] J.D. Callen *et al.*, "Experimental tests of paleoclassical transport," 2006 IAEA Chengdu Fusion Energy Conf. paper EX/P3-2 (submitted to Nucl. Fusion).
[11] J.L. Luxon, Nucl. Fusion **42**, 614 (2002).
[12] G.D. Porter *et al.*, Phys. Plasmas **5**, 1410 (1998).
[13] J. Neuhauser *et al.*, Plasma Phys. Control. Fusion **44**, 855 (2002) — see Fig. 5.
[14] R.J. Groebner *et al.*, Plasma Phys. Control. Fusion **48**, A109 (2006) — see Fig. 3b.
[15] L.D. Horton *et al.*, Nucl. Fusion **45**, 856 (2005).
[16] W.M. Stacey and R.J. Groebner, Phys. Plasmas **13**, 072510 (2006); *ibid.* **14**, 012501 (2007).
[17] W.M. Stacey and T.E. Evans, Phys. Plasmas **13**, 112506 (2006).
[18] A.Y. Pankin *et al.*, Nucl. Fusion **46**, 403 (2006).